Influence of α-Deoxyadenosine on the Stability and Structure of DNA. Thermodynamic and Molecular Mechanics Studies[†]

Hiroshi Ide,*[,‡] Hironori Shimizu,[‡] Yoshiharu Kimura,[‡] Shunji Sakamoto,[‡] Keisuke Makino,[‡] Mary Glackin,[§] Susan S. Wallace,[§] Hiroyuki Nakamuta,[‖] Muneo Sasaki,[‖] and Naoki Sugimoto[‖]

Department of Polymer Science and Engineering, Kyoto Institute of Technology, Matsugasaki, Sakyo-ku, Kyoto 606, Japan, Department of Microbiology and Molecular Genetics, Markey Center for Molecular Genetics, University of Vermont, Burlington, Vermont 05405, and Department of Chemistry, Faculty of Science, Konan University, 8-9-1 Okamoto, Higashinada-ku, Kobe 658, Japan

ABSTRACT: The α anomer of deoxyadenosine (α) and an abasic site (tetrahydrofuran, F), which are DNA lesions produced by free radicals, were site-specifically incorporated in 9-mer duplexes d(TGAGXGTAC)·d-(GTACNCTCA), where X = α or F and N = A, G, C, or T. Their influence on thermodynamic stability and structure of DNA was assessed by UV–melting measurements and molecular mechanics calculations. UV–melting studies revealed that a duplex containing an αT pair was as stable as the parental duplex containing an AT pair at the same site. Furthermore, the stability of duplexes containing α varied depending on the base opposite this lesion, with the T_m decreasing in the following order: αT > αC ≈ αA > αG. On the contrary, an abasic site introduced in the same site showed a significantly greater destabilizing effect than α, but variation of T_m with the bases opposite F was less evident. To delineate the molecular mechanism of the thermodynamic effects of an α lesion, molecular mechanics calculations were performed for the same duplexes as used for UV–melting measurements. The results suggest that the structural perturbation introduced into DNA by an αN pair is αG > αA > αC > αT, showing a parallel correlation with the destabilizing effects of αN pairs. On the basis of these results, it is discussed how the perturbations introduced by these DNA lesions may influence the selection of nucleotides opposite the lesions by DNA polymerases and the interaction with DNA repair enzymes such as *Escherichia coli* endonuclease IV and exonuclease III.

Genotoxic agents such as ionizing radiation, chemical oxidants, and certain antibiotics produce DNA damage via a free radical mechanism (von Sonntag, 1987; Halliwell & Gutterdge, 1989). DNA lesions are generally restored in an error-free way in cells, but if unrepaired, they may be encountered by the DNA replication apparatus. A large body of evidence indicates that free radical induced DNA lesions are differentially processed by the replication and repair machineries depending on their structures. When DNA polymerases encounter a DNA lesion, DNA synthesis can either be arrested by the lesion or proceed past the lesion by translesional synthesis (Ide et al., 1985, 1991; Wallace & Ide, 1990; Evans et al., 1993). These two responses are not mutually exclusive but partially overlapping. In translesional synthesis, selection of a nucleotide opposite the damage is a crucial step in determining the ultimate biological effects of the DNA lesion since insertion of an incorrect nucleotide results in mutation. This is particularly important for multicellular organisms in light of the fact that arrest of DNA replication results merely in the death of a single somatic cell, but accumulation of somatic cell mutations due to error-prone translesional synthesis can lead to tumor initiation or age-related diseases (Ames, 1983; Halliwell & Gutteridge,

1989). However, the precise molecular mechanism of the nucleotide selection at DNA lesions remains to be elucidated. Concerning DNA repair, a number of enzymes that restore free radical induced DNA lesions have been identified and characterized in prokaryotic and eukaryotic cells (Friedberg, 1985; Wallace, 1988; Doetsch & Cunningham, 1990). They specifically recognize the perturbations that DNA lesions introduce into DNA molecules, but the exact chemical nature of the perturbations has not been fully clarified despite the efforts by many laboratories [for example, Kalnik et al. (1988), Vesnaver et al. (1989), Cuniasse et al. (1990), and Kao et al. (1993)].

Recently, we have found that 9-α-2′-deoxy-D-ribofuranosyladenine (α),[1] which is a major adenine lesion produced by hydroxyl radicals under anoxic conditions, is a transient block to DNA synthesis. More importantly, this lesion directs novel misincorporation of nucleotides during translesional synthesis (Ide et al., 1994b). In addition, an enzyme (endonuclease IV) from *Escherichia coli* that recognizes this lesion has been identified (Ide et al., 1994a). Interestingly, endonuclease IV has significantly overlapping substrate specificities with exonuclease III (Wallace, 1988; Doetsch & Cunningham 1990), yet α is recognized only by endonuclease IV. This has raised questions concerning the action

---
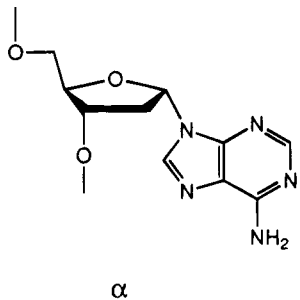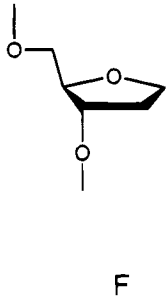
[1] Abbreviations: α, 9-α-2′-deoxy-D-ribofuranosyladenine; F, model abasic site (tetrahydrofuran); T_m, melting temperature; dNTP, deoxyribonucleoside 5′-triphosphate; Pol I, *Escherichia coli* DNA polymerase I Klenow fragment; endo IV, *E. coli* endonuclease IV; exo III, *E. coli* exonuclease III; AP, apurinic/apyrimidinic.

Table 1: Oligodeoxyribonucletide Duplexes Used in This Study

$5'$-T₁ G₂ A₃ G₄ X̲₅ G₆ T₇ A₈ C₉ (strand 1)
$3'$-A₁₈C₁₇T₁₆C₁₅N̲₁₄C₁₃A₁₂T₁₁G₁₀ (strand 2)

X	N	abbreviation	X	N	abbreviation
A	T	AT	α	A	αA
F	A	FA	α	G	αG
F	G	FG	α	C	αC
F	C	FC	α	T	αT
F	T	FT			

mechanism and physiological role of endonuclease IV. In the present study, we have performed UV—melting measurements and molecular mechanics studies on oligodeoxyribonucleotide duplexes containing α to elucidate the perturbations introduced into DNA by the lesion. The data are further compared with those obtained in parallel experiments for an abasic site which is one of the best characterized DNA lesions. We show that the biochemical effects of α and abasic sites on the interaction with DNA polymerases and repair enzymes can be partly correlated with thermodynamic and structural properties of DNA containing these lesions.

EXPERIMENTAL PROCEDURES

Materials. Oligodeoxyribonucleotides containing 9-α-2′-deoxy-D-ribofuranosyladenine (α) or a model abasic site (tetrahydrofuran, F) as well as complementary strands were synthesized using standard solid-phase cyanoethyl phosphoramidite chemistry on a Milligen/Biosearch Cyclone Plus DNA synthesizer. Synthesis and characterization of the phosphoramidite monomers of α and F have been previously reported (Ide et al., 1992, 1993). The oligonucleotides were purified to homogeneity by HPLC, and nucleotide sequences were confirmed as reported (Eritja et al., 1987; Ide et al., 1993). Other reagents were of the highest commercially available grades. Oligonucleotide duplexes used and their abbreviations are listed in Table 1.

UV—Melting Measurements. Absorbance vs temperature melting curves were measured at 260 nm on a Hitachi U-3200 or U-3210 spectrophotometer equipped with a Hitachi SPR-10 temperature controller. The heating rate was 0.5 or 1.0 °C/min. The buffer for the measurement consisted of 1 M NaCl, 10 mM sodium phosphate (pH 7.0), and 1 mM EDTA. The total strand concentration was 1×10^{-5} and 1×10^{-4} M for oligonucleotides containing α and F, respectively. Melting curves were analyzed with a two-state model as described previously (Petersheim & Turner, 1983; Freier et al., 1983).

CD Measurements. CD spectra were obtained on a JASCO J-600 spectropolarimeter equipped with a temperature controller and interfaced to an NEC PC-9801 computer.

The cuvette-holding chamber was flushed with a constant stream of dry N₂ gas to avoid moisture condensation on the cuvette exterior. All CD spectra were measured from 350 to 200 nm in a cuvette with 0.1-cm path length at 5.0 °C. The concentration of samples was 70 μM, and the samples were in a buffer consisting of 1 M NaCl, 10 mM sodium phosphate (pH 7.0), and 1 mM EDTA.

Energy Minimization Calculations. α was constructed from deoxyadenosine and centered in canonical 9-mer B DNA duplexes built using the Biopolymer module of Insight II (version 2.3, Biosym Corp.). To produce a net neutral molecule and to reduce the effects of the high charge density in the phosphate groups of DNA, 18 Na⁺ counterions were placed along the bisector between the phosphate oxygens 2.5 Å from the group. The resultant structures were exhaustively energy minimized to an RMS deviation of ≤ 0.001 kcal/Å² using the molecular mechanics program Discover 2.9 (Biosym Corp.) with AMBER all-atom potentials and partial charges (Weiner et al., 1986). A distance-dependent dielectric constant ($\epsilon = 4$, i.e. $1/4r$) was used to mimic the presence of bulk solvent in the calculation. Energy-minimized structures were calculated for the parental duplex AT and the lesioned duplexes αA, αG, αC, and αT. The resultant structures were displayed in Insight II and analyzed using CURVES (Lavery & Sklenar, 1989ab) and DIALS and WINDOWS (Ravishanker et al., 1989). All calculations were performed on a Silicon Graphics Indigo 2 running IRIX 4.0.5H.

RESULTS

UV—Melting Measurement. Figure 1A shows the UV melting curves of the 9-mer duplexes containing α paired with A, G, C, or T at the central base pair position as well as that of the fully paired parental duplex AT. Incorporation of α altered the duplex stability, and the extent of destabilization relative to the fully paired duplex AT was dependent on the base opposite α. Melting curves of the duplexes in Figure 1A were sigmoidal, exhibiting melting cooperativity. The shapes of the melting curves for the duplexes αA, αG, αC, αT, and AT were analyzed for melting temperature (T_m) and thermodynamic parameters ($\Delta H°$, $\Delta S°$, $\Delta G°_{25}$) for the formation of the duplexes based on a two-state model (Freier et al., 1983). The two-state model is comprised of double-helix and single-strand states (Borer et al., 1974) and has been successfully applied to the analysis of melting behavior of most DNA/DNA and RNA/RNA duplexes (Breslauer et al., 1986; Freier et al., 1986; Sugimoto et al., 1990, 1992, 1994; Sugimoto & Sasaki, 1992). We reasoned that application of this model to the duplexes containing α or F was appropriate on the basis of the following ground. If the melting of the duplexes is a two-state transition, eq 1

$$T_m^{-1} = [R \ln(C_t/n) + \Delta S°]\Delta H° \qquad (1)$$

can be applied (Turner et al., 1990). In eq 1, T_m is the melting temperature of a duplex, $\Delta H°$ and $\Delta S°$ are calculated enthalpy and entropy changes for duplex formation, R is the gas constant, C_t is the total strand concentration, and n reflects the symmetry factor, which is 4 in the present study dealing with non-self-complementary strands. Plots of ln-(C_t/n) vs T_m^{-1} for all the duplexes measured here were linear (data not shown), indicating that the two-state model can be
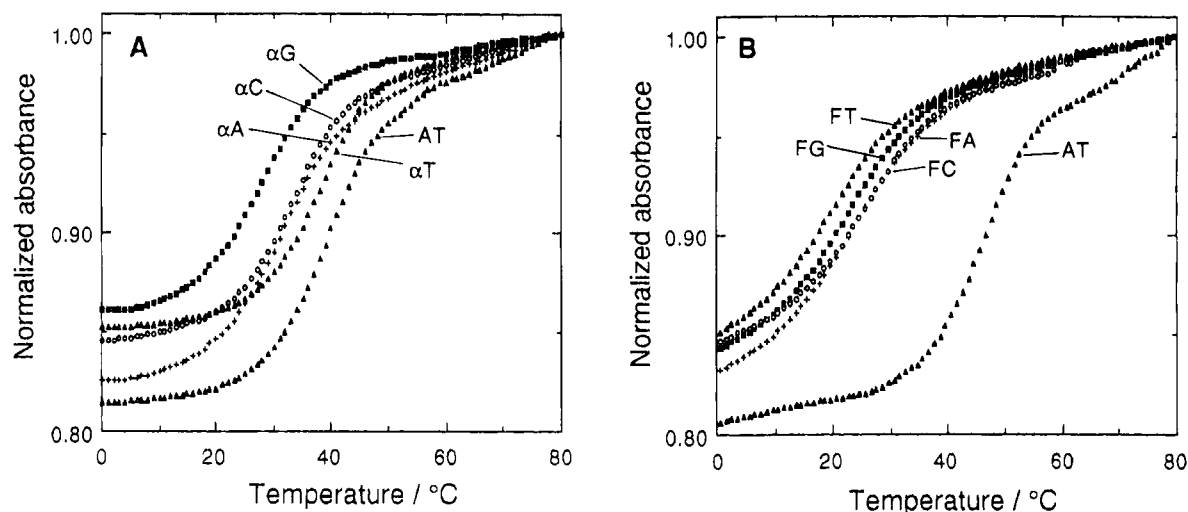
FIGURE 1: UV−melting curves of the duplexes d(TGAGXGTAC)·d(GTACNCTCA), where X = α or F and N = A, G, C, or T: (A) duplexes containing a central αN pair; (B) duplexes containing a central FN pair. A UV−melting curve for the fully paired duplex AT is also shown. The central base pair (XN) is shown for assignment of melting curves. UV−melting curves were measured in 1 M NaCl, 10 mM sodium phosphate (pH 7.0), and 1 mM EDTA with total strand concentrations of 1×10^{-5} and 1×10^{-4} M for duplexes containing α-deoxyadenosine (α) and an abasic site (F), respectively.

Table 2: Thermodynamic Parameters for the Formation of Duplexes Containing α-Deoxyadenosine (α) or a Model Abasic Site (F)[a]

duplex	$-\Delta H°$ (kcal mol^{-1})	$-\Delta S°$ (cal K^{-1} mol)	$-\Delta G°_{25}$ (kcal mol^{-1})	T_m[b] (°C)	ΔT_m[c] (°C)	$\Delta\Delta H°$[c] (kcal mol^{-1})	$\Delta\Delta S°$[c] (cal K^{-1} mol)	$\Delta\Delta G°_{25}$[c] (kcal mol^{-1})
AT	71.6	203	11.0	46.4				
αA	70.3	204	9.33	39.2	−7.2	1.3	-1	1.67
αG	60.8	176	8.36	35.4	−11.0	10.8	27	2.64
αC	66.2	191	9.22	39.0	−7.4	5.4	12	1.78
αT	66.3	186	10.8	47.0	0.6	5.3	17	0.20
FA	44.5	130	5.89	22.5	−23.9	27.1	73	5.11
FG	42.8	123	6.10	23.8	−22.6	28.8	80	4.90
FC	47.6	139	6.32	25.3	−21.1	24.0	64	4.68
FT	57.5	176	5.10	19.0	−27.4	14.1	27	5.90

[a] In 10 mM phosphate buffer (pH 7.0) containing 1 mM EDTA and 1 M NaCl. [b] Melting temperature calculated for total strand concentration = 1×10^{-4} M. [c] Relative to the duplex AT. For example, $\Delta T_m = T_m(XN) - T_m(AT)$ and $\Delta\Delta H° = \Delta H°(XN) - \Delta H°(AT)$, where X = α or F and N = A, G, C, or T.

applied to the melting behaviors of the duplexes containing α or F. The thermodynamic parameters for duplex formation were obtained from eqs 1 and 2 and are listed in Table 2. In

$$\Delta G°_{25} = \Delta H° - 298.15\Delta S° \qquad (2)$$

eq 2, $\Delta G°_{25}$ is the free energy change for the association of the strands at 25 °C. Estimated errors in $\Delta H°$, $\Delta S°$, $\Delta G°_{25}$, and T_m in Table 2 are ±4%, ±4%, ±6%, and ±2%, respectively.

The T_m data in Table 2 indicate that, despite of the potential loss of canonical Watson−Crick base pairing at the central α site, the duplex αT is slightly more stable than the fully paired parental duplex AT. The increase in T_m of the αT pair was 0.6 °C relative to the duplex AT. In contrast, the αA, αG, and αC pairs introduced into the same site destabilized the duplexes, with the destabilizing effect (ΔT_m) ranging 7.2 (αA) to 11.0 °C (αG). Thus, stability of the duplexes containing α was decreased in the following order: αT > αC ≈ αA > αG. The UV−melting curves of the duplexes containing F are shown in Figure 1B. Irrespective of the base opposite F, the duplexes containing F exhibited similar melting profiles, and incorporation of F into the duplexes resulted in a significant reduction of the T_m. The extent of T_m reduction (ΔT_m) by F was much more pronounced as compared with α and ranged from 21.1 to

27.4 °C relative to the fully paired duplex AT. Variation of T_m with the base opposite F was less evident than that with α.

CD Spectra. Figure 2 shows CD spectra of the duplexes containing α or F as well as the parental duplex AT. Both duplexes αN and FN (N = A, G, C, or T) gave CD spectra similar to that of the fully paired duplex AT at 5°C in 1 M NaCl. These data suggest that the duplexes did not undergo global conformational changes such as transitions to A or Z forms due to the incorporation of the lesions at low temperatures.

Molecular Modeling. To evaluate the contributions of the interactions between α and the surrounding bases to the thermodynamic stability and structure of DNA, canonical B DNA oligomers were built with nucleotide sequences identical to those used for UV−melting measurements and exhaustively energy minimized. With the parental duplex AT, a propeller twist (θ_P) of −26° was observed for the central base pair AT, with similar values for the surrounding base pairs, suggesting that the structure of the duplex AT slightly deviates from canonical B DNA (Figure 3). Similar negative propeller twists for AT base pairs have been reported in the X-ray diffraction studies of DNA [for example, Edwards et al. (1992) and Chandrasekaran et al. (1994)]. The buckle, tilt (θ_T), and roll (θ_R) parameters for
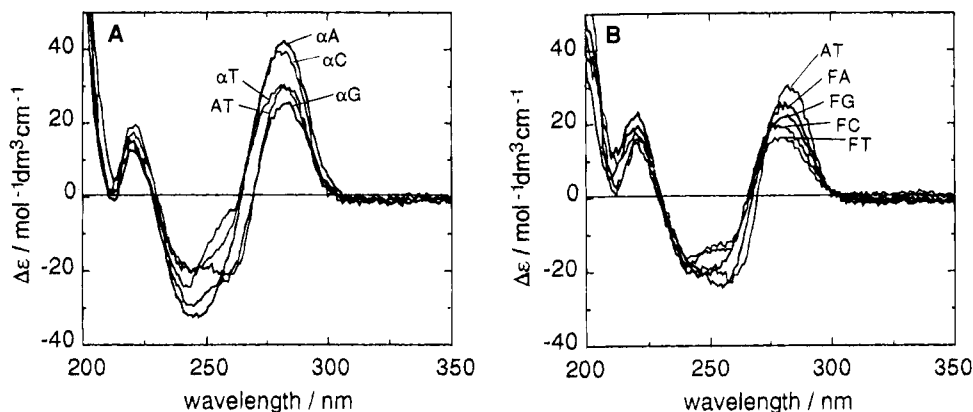
FIGURE 2: CD spectra of the duplexes d(TGAGXGTAC)·d(GTACNCTCA), where X = α or F and N = A, G, C, or T: (A) duplexes containing a central αN pair; (B) duplexes containing a central FN pair. The central base pair (XN) is shown for assignment of CD spectra. CD spectra were measured in 1 M NaCl, 10 mM sodium phosphate (pH 7.0), and 1 mM EDTA with the total strand concentration of 7 × 10^{-5} M at 5 °C.
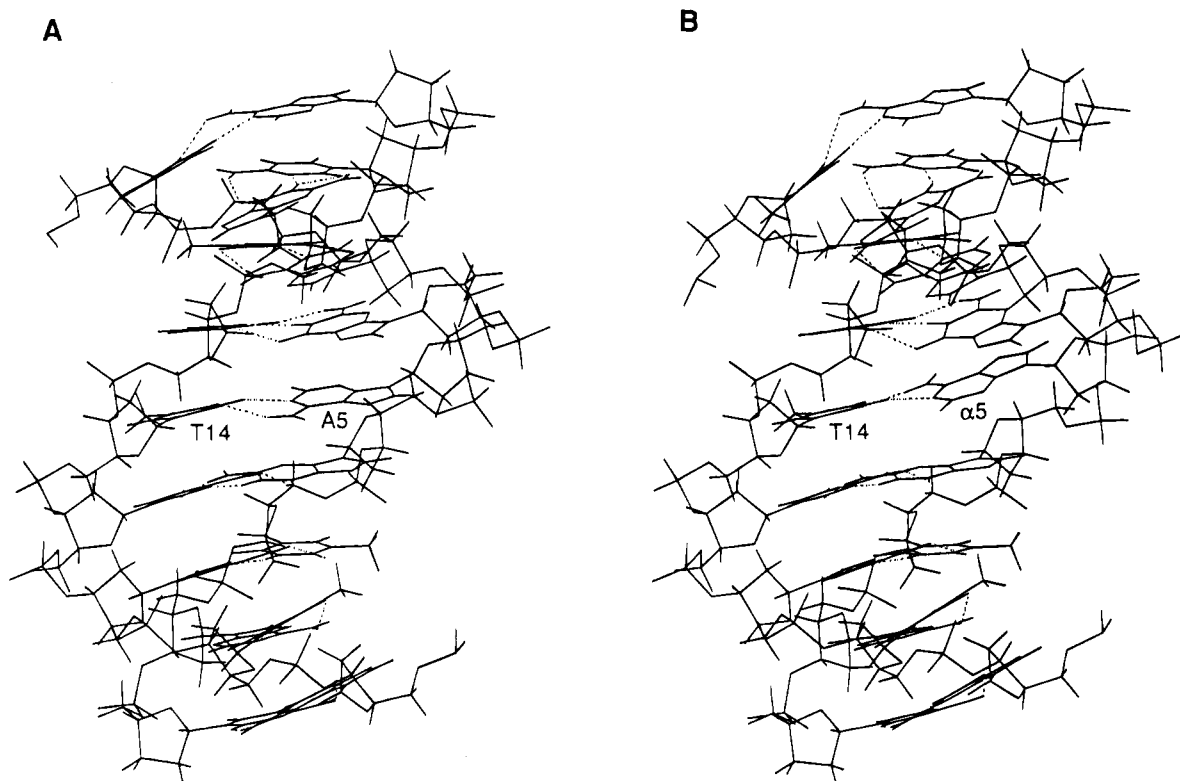

FIGURE 3: Calculated minimum energy structures for the duplexes d(TGAGXGTAC)·d(GTACNCTCA): (A) fully paired parental duplex AT (X = A, N = T): (B) duplex αT (X = α, N = T). The central base pair is indicated by A5·T14 or α5·T14. The duplexes were built using the Biopolymer module of Insight II and exhaustively energy minimized by the molecular mechanics program Discover 2.9 with AMBER parameters. Hydrogen bonds between the paired bases are indicated by dotted lines. Duplexes are viewed from the minor groove.
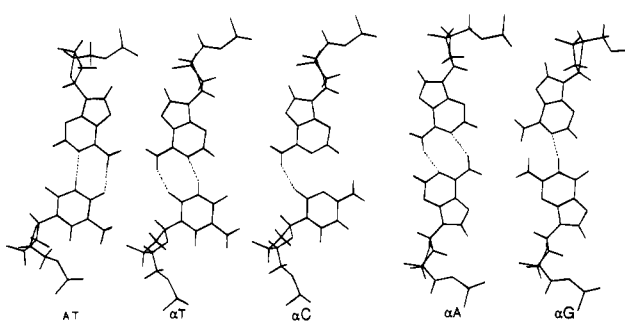
the central base pair are also somewhat larger than those expected for canonical B DNA.

Replacement of A with α causes the adenine ring to protrude in the minor groove with the N6 amino group projecting well into that groove. In the minimized structures, introduction of α changes the glycosidic bond angle (χ) from 240° for central A5 in the duplex AT to approximately 150° for α in the duplex αG and 148° in the other three duplexes. The sugar pucker angle (φ) changes from 133° (C1′-exo) for A5 in the duplex AT to approximately 163° (C2′-endo) for α in both duplexes αC and αT, 218° (C3′-exo) in αG, and 239° (C3′-exo) in αA. The P—O3′ bond angle (ζ) is also altered upon the introduction of α from 262° for A5 in the duplex AT to 228° for α in the duplexes αC and αT and 281° in αG, while remaining almost unaltered in αA (268°).

The helicoidal parameters for all duplexes containing the lesion are also increased compared with the parental duplex AT.

The αT base pair is able to form two hydrogen bonds almost equivalent in distance and angle values to the canonical AT base pair, although the second hydrogen bond is between N6 of α and O2 of the opposing T14 (Figures 3B and 8, Table 3). More importantly, the overall calculated structure of the duplex αT is virtually identical to that of the parental duplex AT (Figure 4A); stacking interactions, base-pairing interactions, and other helical parameters are maintained with values close to those found in the energy-minimized structure of the duplex AT. However, replacement of A with α does move the N6 amino group of α well into the minor groove, and this is accompanied by a slight

Table 3: Calculated Hydrogen Bond Parameters Involving Atoms in the Central Base Pair

duplex	donor[a]	acceptor[a]	distance (Å)	angle (deg)
AT	A5(N6)	T14(O4)	2.1	156.6
	T14(N3)	A5(N1)	1.9	158.9
αA	α5(N6)	A14(N1)	2.1	152.4
	A14(N6)	α5(N1)	2.2	145.0
αC	α5(N6)	C14(O2)	2.0	147.7
	C14(N4)[c]	G4(O6)[b,c]	2.2	139.1
	C15(N4)[b,c]	G4(O6)[b,c]	2.2	139.6
αG	G14(N1)	α5(N1)	2.1	144.8
αT	α5(N6)	T14(O2)	2.0	150.5
	T14(N3)	α5(N1)	2.1	150.1

[a] Atoms participating in hydrogen bond formation are indicated in parentheses. [b] Bifurcated hydrogen bond. [c] Not the central base pair.

shift of the opposing T14 toward the inside of the helix (Figure 4B). A minor displacement of the sugar—phosphate backbone occurs at the lesion site and G4 immediately 5′ to α (Figure 4A). Conversion to α also interrupts base-stacking interactions particularly, in this sequence context, between the adenine of α and G4 locating 5′ to this lesion (Figure 5).

The duplex αC minimizes to a structure almost identical to the duplex αT (Figure 6). Upon superposing the base pairs on either side of the lesion site, the RMS deviation for both structures is less than 0.5 Å. However, alteration of the relative positions of the functional groups on C14 leads to formation of a bifurcated hydrogen bond between the O6 of G4 on strand 1 and N4s of both C14 and C15 on strand 2 (Figure 6 and Table 3). There is also a large axis junction parameter (AIN = 126°) compared with 0° for the duplex AT. This structural change could destabilize the double-helical structure of the molecule, thereby reducing the T_m of this duplex in solution. However, molecular dynamics calculations would be required to confirm such a supposition.

The calculated structure of the duplex αA is remarkably stable considering the introduction of a purine opposite a purine in duplex DNA. Two stable hydrogen bonds are formed between the paired adenines (Table 3). The glycosidic bond angle (χ) does change from 229° for central T14 in the parental duplex AT to 261° for central A14 in the duplex αA, and the sugar pucker angle (φ) concomitantly decreases to 153° (A14) from 120° (T14 in the duplex AT). φ is also altered for G4 locating immediately 5′ to the lesion on strand 1 from 129° to 43° and for C13 (strand 2) opposite G6 from 121° to 48°. Superposition of the structures of the duplexes αA and αT shows the displacement of sugar and bases at the lesion site and the realignment of the DNA backbone (data not shown). The helicoid parameter TIP is increased to −63° at the lesion. Comparison of the two structures of the duplexes αT and αA in Figure 7 indicates
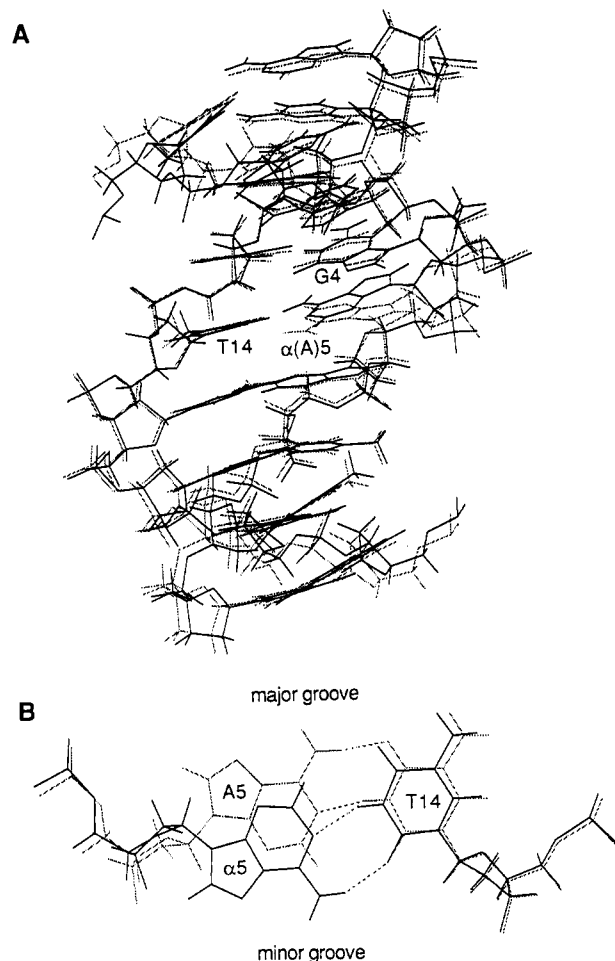
A

major groove

B

minor groove

FIGURE 4: Comparison of the structures for duplex AT and αT with the base pairs immediately 5′ and 3′ to the central base pair (AT or αT) superposed: (A) superposed structures for duplex AT (dotted line) and duplex αT (solid line) viewed from the minor groove; (B) superposed central base pairs AT in duplex AT (dotted line) and αT in duplex αT (solid line) viewed along the helical axis.

that the overall result of these changes in helicoid parameters is a displacement of the DNA backbone at the lesion site and a change in the helical repeat.

Of all four lesioned structures, the duplex αG exhibits the largest distortion from the starting canonical B DNA. Bases on both sides of the lesions are displaced, and the DNA backbone is realigned (Figure 7). The αG base pair is capable of forming only one hydrogen bond between the N1 of G14 and the N1 of α (Table 3). The TIP parameter at the central base pair (91°) shows a large increase relative to those for the duplex AT (0.2°) or the other three lesioned duplexes having negative TIP values. The propeller twist (θ_P) is −51° at the base pair (G4·C15) immediately 5′ to the lesion and 129° at the αG base pair. These are the largest values for any structure in this study. As shown by the ribbon traces in Figure 7, these changes produce a distinct kink in the sugar—phosphate backbone of strand 1 at the α site and a corresponding bulge in the backbone of strand 2.

Preliminary calculations on the duplexes containing F have not produced similar agreement with the biological or thermodynamic data. This is probably due to the parameters used to model F. Further calculations are currently in progress to explore a more appropriate parameter set.
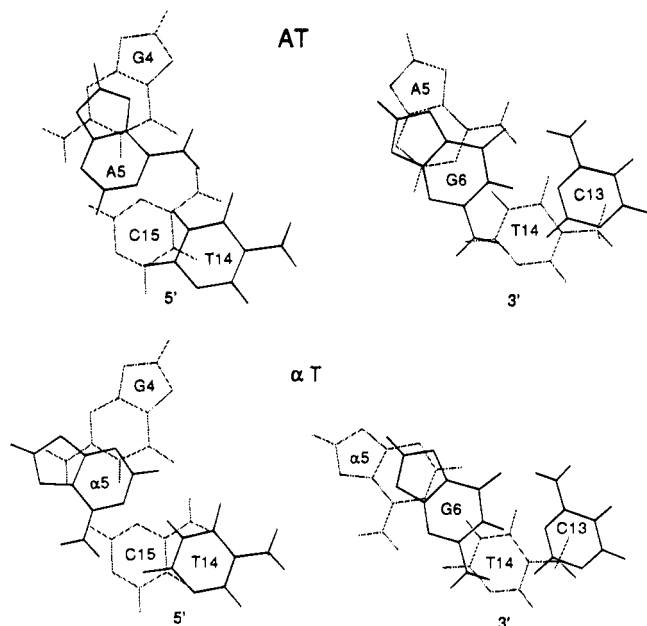
FIGURE 5: Base stacking of the central base pairs in duplexes AT (top two figures) and αT (bottom two figures). Bases are viewed from the 3′ end of strand 1. In the figures labeled 5′, the central A5•T14 or α5•T14 pair (solid line) is stacked on top of the 5′ G4•C15 pair (dotted line), while in the figures labeled 3′, the 3′ G6•C13 pair (solid line) is above the central AT or αT pair (dotted line). Note that the presence of α in this sequence context reduces base-stacking interaction particularly with 5′ flanking G4 (bottom left).
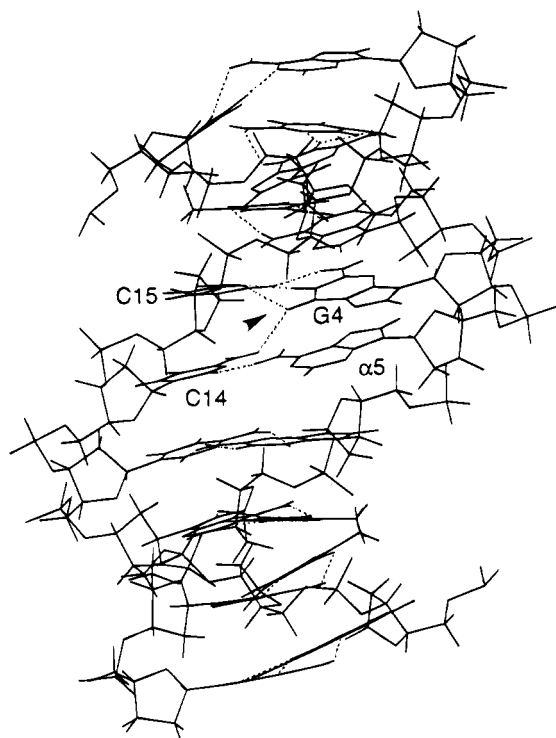

FIGURE 6: Calculated minimum energy structure for duplex αC [d(TGAGαGTAC)•d(GTACCCTCA)]. The central base pair is indicated by α5 and C14. The bifurcated hydrogen bond formed between G4 immediately 5′ to α5 and two C's (C14 and C15) is indicated by an arrow.

DISCUSSION

In the present study, the α anomer of deoxyadenosine (α) and a model abasic site (tetrahydrofuran, F) were site-specifically incorporated in the middle of 9-mer duplexes,

and their influence on the stability of DNA was assessed by UV—melting measurements. These studies revealed that a duplex containing an αT pair was as stable as the fully paired duplex containing an AT pair at the same site. Interestingly, the stability of the duplexes containing α was dependent on the base opposite this lesion and decreased in the following order: αT > αC ≈ αA > αG. In contrast, an abasic site introduced in the same site showed a significantly greater destabilizing effect than α, but variation of T_m with the bases opposite F was less evident. Analysis of the thermodynamic parameters (Table 2) suggests that the increase in $\Delta G°_{25}$ leading to destabilization of the duplexes containing α or F (except for duplex αT) is attributable to an enthalpy factor. The difference in enthalpy changes ($\Delta\Delta H°$) associated with the replacement of a lesion X (α or F) for A is consistently larger than those in the corresponding entropy factors ($T\Delta\Delta S°$), where $\Delta\Delta H° = \Delta H°(XN) - \Delta H°(AT)$ and $\Delta\Delta S° = \Delta S°(XN) - \Delta S°(AT)$. Accordingly, the overall contribution of the enthalpy and entropy factors ($\Delta\Delta H° - T\Delta\Delta S°$) to the free energy changes is positive, thereby resulting in destabilization of the duplexes containing α or F. However, with the duplex αT, the contributions of these two factors are mutually compensated, and the duplex remains as stable as the parental duplex AT.

To delineate the molecular mechanism of the thermodynamic effects of an α lesion in DNA, canonical B DNA models were built with the nucleotide sequences identical to those used for the UV—melting measurements and exhaustively energy minimized. Although energy minimizations may not be expected to completely reproduce the experimental results since they sample only one static conformation of a dynamic molecule and are conducted in the absence of explicit solvent, these calculations can suggest testable structural features of the α lesion in DNA which may contribute to the observed behavior of the DNA duplexes in solution. The calculated structures for the duplexes containing α are in good agreement with the UV—melting data and suggest some structural reasons for the different stabilities of the lesioned duplexes. Although the CD data indicate that all four duplexes, αA, αG, αC, and αT, studied here can assume a B conformation at low temperatures, the energy minimization data suggest that precise positioning of the base and sugar—phosphate backbone deviates from the canonical one. For the duplexes containing an α•pyrimidine pair (αT and αC), the displacement of the sugar—phosphate backbone from the canonical position is relatively minor (Figures 4 and 6). The distortion is localized primarily in the close proximity to the lesion. A notable difference between the two duplexes is that the αT pair forms two hydrogen bonds, one of which is not a canonical one, between N6 of α and O2 of the opposing T, while the αC pair forms a single hydrogen bond (Table 3). The C opposite α also forms an unusual bifurcated hydrogen bond with G4 5′ to α (Figure 6 and Table 3). In addition, the duplex αC has a large axis junction parameter (AIN) potentially leading to destabilization of this duplex. The duplexes containing an α•purine pair (αA and αG) exhibit a large displacement of the sugar—phosphate backbone as well as bases (Figure 7). The distortion is not localized at the lesion site but extends to the surrounding sequences as judged by large alteration of the structural parameters such as the glycosidic bond angle and propeller twist. The duplex αG shows a large TIP parameter and propeller twist at the central
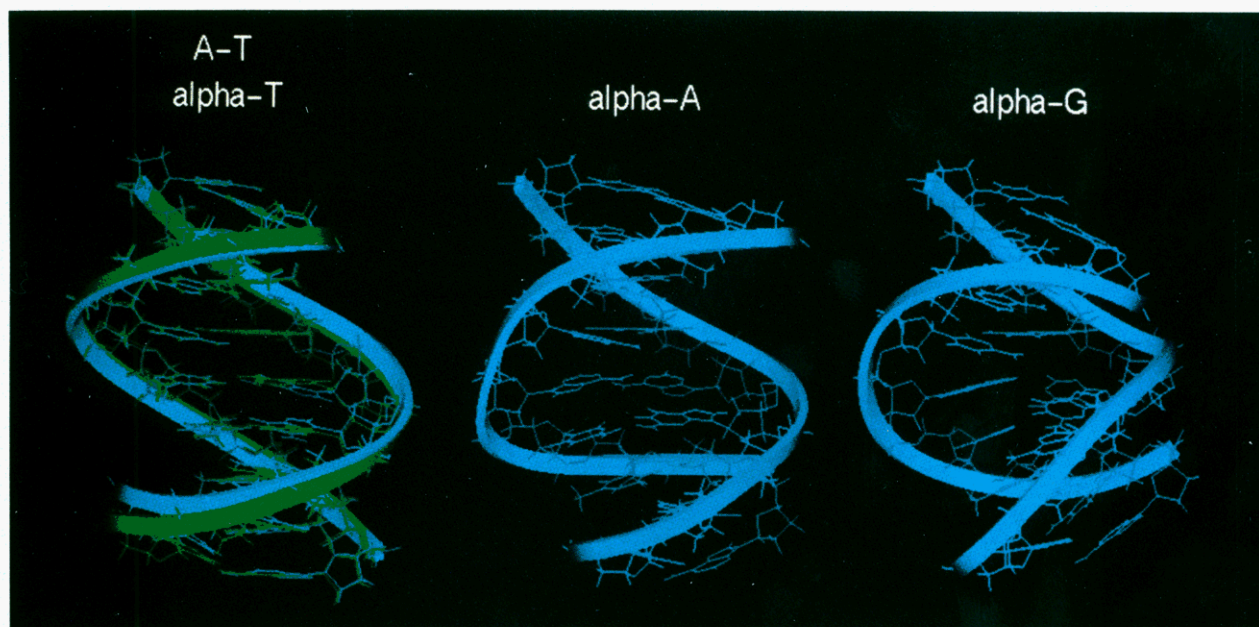
FIGURE 7: Comparison between minimum energy structures for duplexes AT, αT, αA, and αG with solid ribbon traces of the sugar phosphate backbone: duplex AT (left, green), αT (left, blue), αA (center), and αG (right).

αG pair, which produce a distinct kink and a bulge in the DNA backbones. These molecular mechanics data indicate that the extent of perturbations introduced into DNA by the central αN pairs (N = A, G, C, or T) is αG > αA > αC > αT. This order essentially parallels the destabilizing effect (ΔT_m) of the αN pairs on the thermal disruption of the duplexes (αG > αA ≈ αC > αT).

Influence of α-Deoxyadenosine and Abasic Sites on DNA Replication. To achieve extremely high fidelity of DNA replication by DNA polymerases, several check points have been proposed for discrimination between correct and incorrect base pairs (Echols & Goodman, 1991; Johnson, 1993). These occur in the initial substrate (dNTP) binding stage, subsequent conformational change of DNA polymerases, and finally the formation of a phosphodiester bond. In all stages, the discrimination uses precise Watson–Crick geometry of a dNTP–DNA complex, and fine tuning of the geometry is achieved by hydrogen bonding between bases in dNTP and the template, nearest neighbor base stacking, and nonspecific dNTP binding to the triphosphate binding site. The present molecular modeling data have demonstrated that introduction of α in place of A introduces distortions in DNA. When the thermodynamic and molecular mechanics data are taken into account for the response of DNA polymerases that encounter α in the template, it is very likely that altered hydrogen-bonding and stacking interactions as well as displacement of the sugar–phosphate backbone do not allow fine tuning of the geometry of an incoming substrate dNTP, thereby rejecting the substrate in one (or all) of the check points. This results in blocking of DNA synthesis at the site of template α (Ide et al., 1994b). The αT pair can potentially form two hydrogen bonds and has a negligible destabilizing effect on the duplex. However, as indicated by molecular modeling data (Figure 4), the adenine base of α projects deeply into the minor groove, and the positions of the sugar–phosphate backbone of α and the 5′ nucleotide (G4) slightly deviate from the canonical positions. These modifications could cause unfavorable interaction(s) between the template and DNA polymerase

upon fine tuning of the geometry to accept incoming dTTP.

Incorporation of a nucleotide opposite α leading to translesional synthesis will occur after many times of nonproductive binding of dNTP substrates to the active site of DNA polymerases. We have recently shown by *in vitro* experiments that the nucleotide incorporation frequency by *E. coli* DNA polymerase I Klenow fragment (Pol I) is almost exclusively T > C ≥ A ≫ G (Ide et al., 1994b). A minor exception (A > T ≥ C ≫ G) occurred when α was flanked by a nearest neighbor pair T(template)·A(primer). The geometric discrimination also appears to play a key role in determination of the relative frequency of nucleotide incorporation opposite α since the observed nucleotide insertion frequency (T > C ≥ A ≫ G) inversely correlates with the structural (G > A > C > T) and thermodynamic (G > A ≈ C > T) perturbations introduced by αN base pairs (N = A, G, C, or T). Currently, we have no plausible explanation for the exception observed with the TA nearest neighbor mentioned above. The role of base stacking interactions at the primer terminus needs to be further examined to account for this particular result.

Abasic sites (F) significantly reduce the stability of the duplexes (Table 2), which is in good agreement with previous studies on duplex oligonucleotides containing a model or real abasic site (Millican et al., 1984; Bertrandt et al., 1989; Vesnaver et al., 1989). Abasic sites show a greater destabilizing effect (ΔT_m: −22.1 to −27.4 °C) than α (0.6 to −11.0 °C). According to the present T_m data, incorporation of A opposite an abasic site should be less favored than G or C since the destabilizing effect (ΔT_m) of the FG or FC pair was smaller than that of the FA pair, though variation of ΔT_m with the base opposite F was relatively small. However, DNA polymerases insert A most frequently when they encounter abasic sites during DNA synthesis *in vitro* and in *E. coli* (Cai et al., 1993, and references therein), although recent studies have shown that there are exceptions in eukaryotic cells [for example, Cabral-Neto et al. (1992), Kamiya et al. (1992), and Kunz et al. (1994)]. This is also the case for noninstructive DNA lesions such as pyrimidne

ring fragmentation products (Ide et al., 1991; Evans et al., 1993). In addition, there is no apparent parallel correlation between the order of nucleotide insertion frequency opposite F (A > G > T ≈ C) (Cai et al., 1993, and references therein) and that of the destabilizing effect of the FN pair determined in this study (T > A > G > C). It is likely that, in the case of abasic sites or the other noninstructive lesions, the geometric recognition is virtually impaired by the loss of hydrogen-bonding and altered stacking interactions between bases of the substrate dNTP and DNA. As a result, nucleotides are incorporated opposite abasic sites primarily following the default mechanism inherent to DNA polymerases. Thus, it is deduced that the nucleotide selection at DNA lesions is driven by two distinct mechanisms. One is the geometric recognition which is predominantly operating for a DNA lesion like α. Probably this mechanism is also dominant for lesions such as thymine glycol (Ide et al., 1985; Hayes et al., 1988), dihydrothymine (Ide et al., 1991), 8-oxoguanine (Shibutani et al., 1991), and 8-oxoadenine (Wood et al., 1992), which potentially retain some hydrogen-bonding and/or stacking abilities. If the geometric recognition is impaired by gross alteration of base structures such as for abasic sites (Cai et al., 1993, and references therein) or pyrimidine ring fragmentation products (Ide et al., 1991; Evans et al., 1993), the default mechanism inherent to DNA polymerase becomes dominant.

Substrate Specificities of E. coli Exonuclease III and Endonuclease IV. A number of AP endonucleases have been identified and characterized in prokaryotes and eukaryotes. *E. coli* exonuclease III (exo III) and endonuclease IV (endo IV) are among the enzymes that have been most extensively studied (Wallace, 1988; Doetsch & Cunningham, 1990). They are class II AP (nucleotidyl hydrolases) and hydrolytically cleave the phosphodiester bond 5′ to abasic sites. Exo III is a major constitutive AP endonuclease and accounts for about 90% of AP endonuclease activity in *E. coli* cells (Ljungquist et al., 1976; Cunningham et al., 1986), while endo IV is an enzyme inducible by redox recycling agents (Chan & Weiss, 1987). In addition to the AP endonuclease activity (Warner et al., 1980; Mosbaugh & Linn, 1980), these two enzymes have significantly overlapping substrate specificities including urea N-glycosides (Kow & Wallace, 1985; Wallace et al., 1988), alkylhydroxylamine-modified abasic sites (Kow, 1989), and 3′-blocking damages (Miwa & Moses, 1981; Mosbaugh & Linn, 1982; Demple et al., 1986) (Table 4) despite an apparent lack of primary amino acid sequence homology (Saporito et al., 1988; Saporito & Cunningham, 1988). The significant overlap in the substrate specificities of exo III and endo IV has raised questions concerning the physiological role of endo IV. Recently, we have shown that endo IV specifically recognizes α in duplex DNA and cleaves the phosphodiester bond 5′ to this lesion (Ide et al., 1994a). However, this lesion is not recognized by exo III or class I AP endonucleases (AP lyases). These results suggest that endo IV may be involved in the repair of a new class of DNA damages that are not recognized by the other repair enzymes.

The substrates recognized by endo IV as well as exo III (type 2 lesions in Table 4) have a common feature, which is a space in the vicinity of the 5′-flanking phosphodiester or monoester bond in the major groove. With the type 4 lesions that are not recognized by either exo III or endo IV, the space is occupied by damaged bases projecting into the major

Table 4: Substrate Specificities of Exo III and Endo IV

type	substrate[a]	activity[b] exo III	activity[b] endo IV
1	3′-terminal nucleotide (3′-5′ exonuclease)	○	×
2	deoxyribose 5-phosphate[c]	○	○
	4-hydroxy-2-pentanal residue[c]	○	○
	phosphoglycol aldehyde ester[c]	○	○
	phosphoglycolate residue[c]	○	○
	phosphate[c]	○	○
	abasic site	○	○
	urea N-glycoside	○	○
	alkylhydoxylamine N-glycoside	○	○
3	α-deoxyadenosine	×	○
4	β-ureidoisobutyric acid	×	×
	formamidopyrimidine	×	×
	thymine glycol	×	×
	dihydrothymine	×	×

[a] In duplex DNA. [b] ○ indicates that the lesion is a substrate for the enzyme, while × is not. [c] 3′-terminal lesions.

groove. On the basis of this feature, Weiss (1976, 1981) and later on Kow (1989) have proposed that exo III uses this space for the recognition of damages and/or catalytic activity. It is likely that endo IV also uses this feature for its activity since type 2 lesions are recognized by endo IV as well as exo III. Furthermore, this is consistent with the present molecular modeling data that the major groove around α becomes deeper relative to that of the normal duplex AT (Figure 4B), thereby creating a space in close proximity to the 5′-flanking phosphodiester bond to be cleaved by endo IV. The question then arises why exo III does not act on α if the model proposed by Weiss and Kow is correct. The present UV−melting studies show that the duplexes containing an abasic site (type 2 lesion) or α (type 3 lesion) have different stabilities. Although the destabilizing effects on melting temperature of the type 2 lesions other than abasic sites have not been determined, it is reasonable to assume that they will be in a comparable range with those observed for abasic sites since their structures imply complete loss of hydrogen bonding and stacking. Thus, in DNA, the flanking regions of type 2 lesions, whether embedded in 3′-terminal or internal positions, have considerably large conformational flexibilty. This will result in local melting or unwinding of DNA. NMR studies on internal abasic sites (Cuniasse et al., 1990) and terminal nucleotides (Pardi & Tinoco, 1982) also support this conformational flexibility. In contrast, those surrounding α (type 3 lesion) retain a more tight duplex structure than type 2 lesions as judged by T_m. Accordingly, it is tempting to speculate that exo III requires both the space in close proximity to the target phosphate and conformational flexibility for the enzymatic activity, while the conformational flexibility is not a absolute requirement for endo IV, and the space is sufficient for the enzymatic action. Possible roles for the space in the action of endo IV include (i) sensing the lesion that allows tight binding of the enzyme to DNA, (ii) removal of a steric hindrance that facilitates nucleophilic attack on the target phosphate atom, and (iii) ligand coordination to the target phosphate oxygen atoms that stabilizes the transition state.

REFERENCES

Ames, B. N. (1983) *Science 221*, 1256−1264.

Bertrandt, J.-R., Vasseur, J.-J., Rayner, B., Imbach, J.-L., Paoletti, C., & Malvy, C. (1989) *Nucleic Acids Res. 17*, 10307−10319.

Borer, P. N., Dengler, B., Tinoco, I., Jr., & Uhlenbeck, O. C. (1974) *J. Mol. Biol. 86*, 843−853.

Breslauer, K. J., Frank, R., Bloecker, H., & Marky, L. A. (1986) *Proc. Natl. Acad. Sci. U.S.A. 83*, 3746−3750.

Cabral-Neto, J. B., Gentil, A., Casiera Cabral, R. E., & Sarasin, A. (1992) *J. Biol. Chem. 267*, 19718−19723.

Cai, H., Bloom, L. B., Eritja, R., & Goodman, M. F. (1993) *J. Biol. Chem. 268*, 23567−23572.

Chan, E., & Weiss, B. (1987) *Proc. Natl. Acad. Sci. U.S.A. 84*, 3189−3913.

Chandrasekaran, R., Radha, A., & Ratliff, R. L. (1994) *J. Biomol. Str. Dyn. 11*, 741−765.

Cuniasse, P., Fazakerley, G. V., Gushlbauer, W., Kaplan, B. E., & Sowers, L. C. (1990) *J. Mol. Biol. 213*, 303−314.

Cunningham, R. P., Saporito, S. M., Spitzer, S. G., & Weiss, B. (1986) *J. Bacteriol. 168*, 1120−1127.

Demple, B., Johnson, A., & Fung, D. (1986) *Proc. Natl. Acad. Sci. U.S.A. 83*, 7731−7735.

Doetsch, P. W., & Cunningham, R. P. (1990) *Mutat. Res. 235*, 173−201.

Echols, H., & Goodman, M. F. (1991) *Annu. Rev. Biochem. 60*, 477−511.

Edwards, K. J., Brown, D. G., Spink, N., Skelly, J. V., & Neidle, S. (1992) *J. Mol. Biol. 226*, 1161−1173.

Eritja, R., Walker, P. A., Randall, S. K., Goodman, M. F., & Kaplan, B. E. (1987) *Nucleosides Nucleotides 6*, 803−814.

Evans, J., Maccabee, M., Hatahet, Z., Courcelle, J., Bockrath, R., Ide, H., & Wallace, S. S. (1993) *Mutat. Res. 299*, 147−156.

Freier, S. M., Burger, B. J., Alkema, D., Neilson, T., & Turner, D. H. (1983) *Biochemistry 22*, 6198−6206.

Freier, S. M., Kierzek, R., Jaeger, J. A., Sugimoto, N., Caruthers, M. H., Neilson, T., & Turner, D. H. (1986) *Proc. Natl. Acad. Sci. U.S.A. 83*, 9373−9377.

Friedberg, E. C. (1985) *DNA Repair*, W. H. Freeman, New York.

Halliwell, B., & Gutteridge, J. M. (1989) *Free Radicals in Biology and Medicine*, Oxford University Press, Oxford.

Hayes, R. C., Petrullo, L. A., Huang, H., Wallace, S. S., & LeClerc, J. E. (1988) *J. Mol. Biol. 201*, 239−246.

Ide, H., Kow, Y. W., & Wallace, S. S. (1985) *Nucleic Acids Res. 13*, 8035−8052.

Ide, H., Petrullo, L. A., Hatahet, Z., & Wallace, S. S. (1991) *J. Biol. Chem. 266*, 1469−1477.

Ide, H., Murayama, H., Murakami, A., Morii, T., & Makino, K. (1992) *Nucleic Acids Res. Symp. Ser. 27*, 167−168.

Ide, H., Okagami, M., Murayama, H., Kimura, Y., & Makino, K. (1993) *Biochem. Int. 31*, 485−491.

Ide, H., Tedzuka, K., Shimizu, H., Kimura, Y., Purmal, A. A., Wallace, S. S., & Kow, Y. W. (1994a) *Biochemistry 33*, 7842−7847.

Ide, H., Yamaoka, T., & Kimura, Y. (1994b) *Biochemistry 33*, 7127−7133.

Johnson, K. A. (1993) *Annu. Rev. Biochem. 62*, 685−713.

Kalnik, M. W., Chang, C. N., Grollman, A. P., & Patel, D. J. (1988) *Biochemistry 27*, 924−931.

Kamiya, H., Suzuki, M., Komatsu, Y., Miura, H., Kikuchi, K., Sakaguchi, T., Murata, N., Masutani, C., Hanaoka, F., & Ohtsuka, E. (1992) *Nucleic Acids Res. 20*, 4409−4415.

Kao, J. Y., Goljer, I., Phan, T. A., & Bolton, P. H. (1993) *J. Biol. Chem. 268*, 17787−17793.

Kow, Y. W. (1989) *Biochemistry 28*, 3280−3287.

Kow, Y. W., & Wallace, S. S. (1985) *Proc. Natl. Acad. Sci. U.S.A. 82*, 8354−8358.

Kunz, B. A., Henson, E. S., Roche, H., Ramotar, D., Nunoshiba, T., & Demple, B. (1994) *Proc. Natl. Acad. Sci. U.S.A. 91*, 8165−8169.

Lavery, R., & Sklenar, H. (1989a) *J. Biomol. Struct. Dyn. 6*, 63−91.

Lavery, R., & Sklenar, H. (1989b) *J. Biomol. Struct. Dyn. 6*, 655−667.

Ljungquist, S., Lindahl, T., & Howard-Flanders, P. (1976) *J. Bacteriol. 126*, 646−653.

Millican, T. A., Mock, G. A., Chauncey, M. A., Patel, T. P., Eaton, M. A. W., Gunning, J., Cutbush, S. D., Neidle, S., & Mann, J. (1984) *Nucleic Acids Res. 12*, 7435−7453.

Miwa, O., & Moses, R. E. (1981) *Biochemistry 20*, 238−244.

Mosbaugh, D. W., & Linn, S. (1980) *J. Biol. Chem. 255*, 11742−11752.

Mosbaugh, D. W., & Linn, S. (1982) *J. Biol. Chem. 257*, 575−583.

Pardi, A., & Tinoco, I., Jr. (1982) *Biochemistry 21*, 4686−4693.

Petersheim, M., & Turner, D. H. (1983) *Biochemistry 22*, 256−263.

Ravishanker, G., Swaminathan, S., Beveridge, D. L., Lavery, R., & Sklenar, H. (1989) *J. Biomol. Struct. Dyn. 6*, 669−699.

Saporito, S. M., & Cunningham, R. P. (1988) *J. Bacteriol. 170*, 5141−5145.

Saporito, S. M., Smith-White, B. J., & Cunningham, R. P. (1988) *J. Bacteriol. 170*, 4542−4547.

Shibutani, S., Takeshita, M., & Grollman, A. P. (1991) *Nature 349*, 431−434.

Sugimoto, N., & Sasaki, M. (1992) *Nucleosides Nucleotides 11*, 515−520.

Sugimoto, N., Hasegawa, K., & Sasaki, M. (1990) *Chem. Express 5*, 249−252.

Sugimoto, N., Shintani, Y., Tanaka, A., & Sasaki, M. (1992) *Bull. Chem. Soc. Jpn. 65*, 535−540.

Sugimoto, N., Honda, K., & Sasaki, M. (1994) *Nucleosides Nucleotides 13*, 1311−1317.

Turner, D. H., Sugimoto, N., & Freier, S. M. (1990) in *Landolt-Bornstein Nucleic Acids* (Saenger, W. R., Ed.) Vol. 1c, Chapter 3.6, Berlin, Germany.

Vesnaver, G., Chang, C., Eisenberg, M., Grollman, A. P., & Breslauer, K. J. (1989) *Proc. Natl. Acad. Sci. U.S.A. 86*, 3614−3618.

von Sonntag, C. (1987) *The Chemical Basis of Radiation Biology*, Taylor & Francis, London.

Wallace, S. S. (1988) *Environ. Mol. Mutagen. 12*, 431−477.

Wallace, S. S., & Ide, H. (1990) in *Ionizing Radiation Damage to DNA* (Wallace S. S., & Painter, R., Eds.) pp 1−15, Wiley-Liss, New York.

Wallace, S. S., Ide, H., Kow, Y. W., Laspia, M. F., Melamede, R. J., Petrullo, L. A., & LeClerc, J. E. (1988) in *Mechanisms and Consequences of DNA Damage Processing* (Friedberg, E. C., & Hanawalt, P., Eds.) pp 151−157, Alan R. Liss, New York.

Warner, H. R., Demple, B. F., Deutach, W. A., Kane, C. M., & Linn, S. (1980) *Proc. Natl. Acad. Sci. U.S.A. 77*, 4602−4606.

Weiner, S. J., Kollman, P. A., Ngyen, D. T., & Case, D. A. (1986) *J. Comput. Chem. 7*, 230−252.

Weiss, B. (1976) *J. Biol. Chem. 251*, 1896−1901.

Weiss, B. (1981) in *The Enzymes* (Boyer, P. D., Ed.) pp 203−231, Academic Press, New York.

Wood, M. L., Esteve, A., Morningstar, M. L., Kuziemko, G. M., & Essigmann, J. M. (1992) *Nucleic Acids Res. 20*, 6023−6932.